School of Natural Sciences and Mathematics

Understanding and Controlling Water Stability of MOF-74

Citation:

Zuluaga, S., E. M. A. Fuentes-Fernandez, K. Tan, F. Xu, et al. 2016. "Understanding and controlling water stability of MOF-74." Journal of Materials Chemistry A 4(14): doi:10.1039/c5ta10416e

Journal of Materials Chemistry A

PAPER

View Article Online
View Journal | View Issue

Cite this: J. Mater. Chem. A, 2016, 4, 5176

Understanding and controlling water stability of MOF-74

Sebastian Zuluaga,[a] Erika M. A. Fuentes-Fernandez,[b] Kui Tan,[b] Feng Xu,[c] Jing Li,[c] Yves J. Chabal[b] and Timo Thonhauser*[a]

Received 19th December 2015
Accepted 8th March 2016

DOI: 10.1039/c5ta10416e

www.rsc.org/MaterialsA

Metal organic framework (MOF) materials in general, and MOF-74 in particular, have promising properties for many technologically important processes. However, their instability under humid conditions severely restricts practical use. We show that this instability and the accompanying reduction of the CO_2 uptake capacity of MOF-74 under humid conditions originate in the water dissociation reaction $H_2O \rightarrow OH + H$ at the metal centers. After this dissociation, the OH groups coordinate to the metal centers, explaining the reduction in the MOF's CO_2 uptake capacity. This reduction thus strongly depends on the catalytic activity of MOF-74 towards the water dissociation reaction. We further show that—while the water molecules themselves only have a negligible effect on the crystal structure of MOF-74—the OH and H products of the dissociation reaction significantly weaken the MOF framework and lead to the observed crystal structure breakdown. With this knowledge, we propose a way to suppress this particular reaction by modifying the MOF-74 structure to increase the water dissociation energy barrier and thus control the stability of the system under humid conditions.

1 Introduction

Metal organic framework (MOF) materials have promising properties towards technologically important applications such as gas storage and sequestration,[1–10] sensing,[11–15] polymerization,[16,17] luminescence,[18,19] non-linear optics,[20] magnetic networks,[21] targeted drug delivery,[22] multiferroics,[23–25] and catalysis.[26–29] In particular, MOF-74 [M_2(dobdc), M = Mg^{2+}, Zn^{2+}, Ni^{2+}, Co^{2+}, and dobdc = 2,5-dihydroxybenzenedicarboxylic acid] exhibits unsaturated metal centers ideal for the adsorption of small molecules such as H_2,[30,31] CO_2,[32–34] N_2,[35] and CH_4,[36] among others. Unfortunately, the presence of water vapor can reduce the gas uptake significantly and can even destroy the crystal structure of several members of the MOF-74 family,[37–41] restricting its practical use. The exact mechanisms responsible for this structural instability and the reduction in the CO_2 gas uptake are poorly understood and their relation is unclear. For example: after Mg–MOF-74 is exposed to humid conditions, its CO_2 gas uptake capacity is severely reduced, while its crystal structure remains intact.[39] On the other hand, Ni–MOF-74 suffers a smaller reduction in CO_2 uptake capacity, but its crystal structure is considerable damaged by water vapor.[39]

A great effort has been made to enhance the stability of MOFs under humid conditions.[42–45] For example, Gao and co-workers obtained two new rht-MOFs (rht-MOF–triazolate and rht-MOF–pyrazolate) that are isostructural with rht-MOF-1, but exhibit an enhancement in their stability under humid conditions.[46] Decoste and co-workers have been able to enhance the stability of Cu–BTC (1,3,5-benzenetricarboxylic acid, BTC) MOF by treating it with plasma-enhanced chemical vapor deposition of perfluorohexane, which results in a hydrophobic form of Cu–BTC with a remarkable stability under humid conditions.[47] Other groups have shown that it is possible to enhance the stability of three micro porous Zn–MOFs by introducing water repellent groups such as methyl, shielding the metal centers from water molecules and thus enhancing the stability of the MOF under humid conditions.[48] Concerning MOF-74, Jiao and co-workers have synthesized and characterized a series of MM–MOF-74 structures, replacing some of the Mg metal centers of Mg–MOF-74 with either Ni or Co atoms.[49] Their results show that the addition of a small amount of Ni (16 mol%) remarkably enhances the water stability of those systems.

As mentioned before, it is not fully understood how the water molecules affect the crystal structure and the adsorption properties of the MOF-74 system. However, some preliminary work has been done on this topic, which inspired our own research. Decoste and co-workers[41] hypothesize that the adsorption of water on the metal centers of Mg–MOF-74 breaks the bonds that bind the one-dimensional channels together and thus hinders the diffusion of small molecules to the interior of the MOF. As

[a]Department of Physics, Wake Forest University, Winston-Salem, North Carolina 27109, USA. E-mail: thonhauser@wfu.edu

[b]Department of Materials Science and Engineering, University of Texas at Dallas, Richardson, Texas 75080, USA

[c]Department of Chemistry and Chemical Biology, Rutgers University, Piscataway, New Jersey 08854, USA

a results, the gas uptake capacity is reduced, but leaves the structure of the channels intact, explaining why X-ray patterns do not show significant changes in the crystal structure of this MOF. Han *et al.*[50] performed molecular dynamics simulations on the adsorption of water on Zn–MOF-74, finding that before it looses its crystal structure, the water molecules dissociate into OH and H at the metal centers. However, further experimental and theoretical work is needed to truly understand this interesting effect.

Only recently, our group has found experimental proof of the dissociation of water at the metal centers of MOF-74 at temperatures above 150 °C,[51,52] where we found first hints concerning the $H_2O \rightarrow OH + H$ reaction and its relation to the CO_2 uptake reduction. In the present work, combining experimental and *ab initio* results, we uncover the exact mechanism that is responsible for the degradation of MOF-74 under humid condition and elucidate the connection between its structural instability and CO_2 uptake decrease. We prove four points concerning the interaction of water with the MOF-74 structure: (i) once the $H_2O \rightarrow OH + H$ reaction takes place, the OH poisons the metal centers of MOF-74 and reduces the CO_2 gas uptake capacity of the system; (ii) H_2O itself has only a negligible effect on the linker–metal bonds—*i.e.* oxygen–metal (O–M), where we consider M = Zn, Mg, Ni, and Co—and the crystal structure of MOF-74. The reaction products OH and H are the ones responsible for the elongation of the O–M bonds and the breakdown of the crystal structure; (iii) different metal centers have different O–M elongations in the presence of OH and H groups. O–Mg and O–Co bonds are the least affected, while O–Zn and O–Ni are the most affected; and finally, (iv) the $H_2O \rightarrow OH + H$ reaction can be suppressed by an appropriate linker modification.

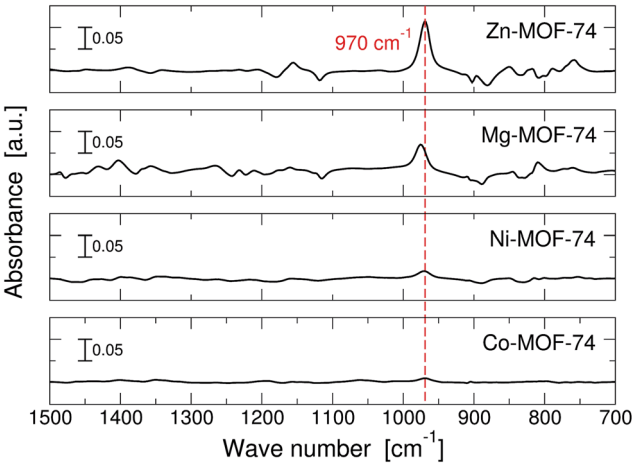

Fig. 1 IR absorption spectra of Zn–, Mg–, Ni–, and Co–MOF-74 hydrated by introducing 8 Torr of D_2O vapor for 20 minutes at 200 °C, referenced to the activated MOF in vacuum. See the work of Tan and co-workers[51] for more information.

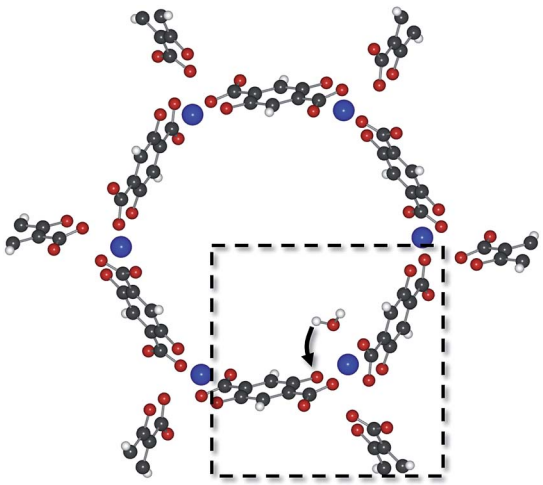

Fig. 2 Graphical representation of MOF-74 and the $H_2O \rightarrow OH + H$ reaction. The hexagonal channel structure of MOF-74 with its six equivalent open metal sites per unit cell is clearly visible. The arrow indicates how the H atom of the water molecule is transferred to the O atom of the linker. Black, red, white, and blue spheres represent C, O, H, and metal atoms. The box indicates the portion of MOF-74 visible in Fig. 5, albeit from a slightly different angle.

2 Results and discussion

2.1 Fingerprint of the $H_2O \rightarrow OH + H$ reaction

Until recently, experiments have not been able to detect the $H_2O \rightarrow OH + H$ reaction in MOF-74.[37–41] Our group was the first to detect its fingerprint in form of a sharp peak in the IR spectrum of Zn–MOF-74 at 970 cm^{-1}, which can only be observed when the MOF is exposed to D_2O above 150 °C; for H_2O, this mode is at 1316 cm^{-1}, where it strongly couples to and gets drowned by modes of the linker, making it impossible to detect.[51,52] For this reason, we conducted our experiments in the present study with D_2O instead of H_2O. Although, for simplicity, throughout the text we may still use the word "water" or "H_2O". Furthermore, for Mg–, Ni–, and Co–MOF-74, the peak is observed at 977 cm^{-1}, 971 cm^{-1}, and 969 cm^{-1} (see Fig. 1), but we will refer to all these peaks as the "970 cm^{-1} peak".

Using *ab initio* simulations, we found the $H_2O \rightarrow OH + H$ reaction to proceed along the following pathway: once the water molecule is adsorbed at the metal center, one of its H atoms is donated to the nearest O of the linker, as depicted in Fig. 2; the activation barrier for this process is 1.02 eV,[51] as discussed in detail below.

2.2 Relation between amount of water dissociated and CO_2 uptake reduction

We now analyze the relationship between the integrated area *A* of the peak at 970 cm^{-1}, which is a direct measure of the amount of water dissociated and the decrease in CO_2 uptake. In Table 1 we show the integrated area of the peak at 970 cm^{-1} and the CO_2 uptake reduction after the M–MOF-74 system (M = Zn, Mg, Ni, and Co) has been exposed to 8 Torr of D_2O vapor at 100 °C and 200 °C. The dissociation reaction starts at 150 °C,[51] so that the reported values for 100 °C and 200 °C are clearly below and above the threshold temperature. The table confirms that a significant reduction in the CO_2 uptake only appears at

Table 1 Integrated area A of the peak at 970 cm^{-1} in the IR spectrum and CO_2 uptake reduction [%] after M–MOF-74 (M = Zn, Mg, Ni, and Co) has been exposed to 8 Torr of D_2O vapor at 100 °C and 200 °C for 20 minutes. This data is also plotted in the top panel of Fig. 3, where its linear relationship becomes obvious. At 100 °C A falls below our level of resolution and we report it as zero

	100 °C		200 °C	
M	CO_2 red.	A	CO_2 red.	A
Zn	8%	0.00	60%	0.09
Mg	7%	0.00	41%	0.06
Ni	2%	0.00	23%	0.03
Co	2%	0.00	9%	0.01

elevated temperatures, *i.e.* once the water dissociation reaction has started. The table also reveals the close relation between the amount of water dissociated at the metal centers (A) and the reduction in CO_2 uptake. In fact, the relationship is almost perfectly linear, as can bee seen in the top panel of Fig. 3. It follows that the dissociation reaction is the key factor controlling the reduction in gas uptake when MOF-74 is exposed to humid conditions: the metal centers of the MOF-74 are being poisoned by the OH groups after the dissociation reaction takes place and are not available for binding CO_2 anymore—or any other small molecules, for that matter.

As evident from Table 1 and Fig. 3, MOFs with different metals show a varying degree of catalytic activity towards the $H_2O \rightarrow OH + H$ reaction. But, what causes and/or determines the catalytic activity towards the water dissociation reaction for a particular metal? Clearly, the catalytic activity is not related to how strong the water binds to the metal centers.[6,54] However, if we plot the catalytic activity (area A under the peak at 970 cm^{-1}) against the calculated radius of the atoms,[53] we obtain a perfectly linear fit, as can be seen in the lower panel of Fig. 3. The reason for this is the following: in the $H_2O \rightarrow OH + H$ reaction, the metal centers interact with the O atom of the water, while one of the H is transferred to the linker, see Fig. 2. In other words, the water molecule interacts with the metal center and the linker at the same time. As the size of the metal centers decreases, the H atoms (of the water molecule) get closer to the O atoms of the linker, increasing the interaction between them and facilitating the transfer of the H to the linker. We thus can use the size of the metal atoms as a predictor of the catalytic activity of the MOF-74 system towards the $H_2O \rightarrow OH + H$ reaction.

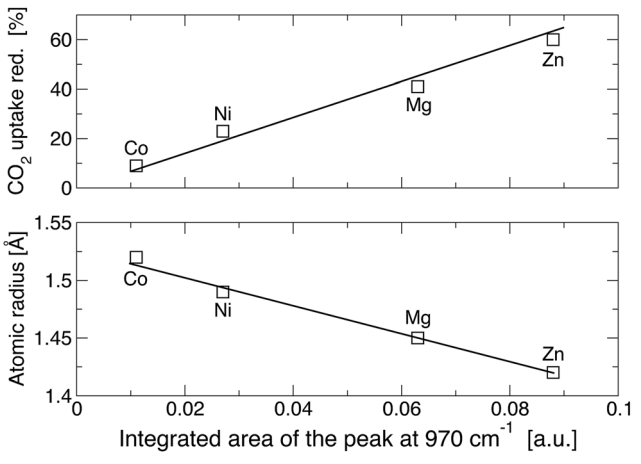

Fig. 3 (top) Reduction in CO_2 uptake as a function of the integrated area A of the peak in the IR spectrum at 970 cm^{-1} in Fig. 1, which is a measure of the amount of water that has dissociated. The reduction is measured after M–MOF-74 (M = Zn, Mg, Ni, and Co) has been exposed to 8 Torr of D_2O vapor at 200 °C for 20 minutes. Data taken from Table 1. (bottom) The radius of the metal centers (Zn, Mg, Ni and Co)[54] *vs.* catalytic activity towards the $H_2O \rightarrow OH + H$ reaction (integrated area A under the peak at 970 cm^{-1}). The straight lines are linear fits to the data.

2.3 Relation to structural stability

According to Table 1, Zn–MOF-74 is the system with the highest catalytic activity towards the dissociation reaction in the MOF-74 family; it also exhibits the largest reduction in CO_2 uptake capacity after being exposed to humid conditions. We will thus use this system to study the effect of water on the crystal structure. To this end, we exposed Zn–MOF-74 for 48 hours to three different conditions: (i) vacuum (less than 20 mTorr) at 300 °C, (ii) 8 Torr of D_2O at 100 °C, and (iii) 8 Torr of D_2O at 300 °C. Fig. 4 shows the corresponding X-ray patterns in panels (b), (c), and (d). Panel (a) serves as the reference and shows the X-ray pattern of the pristine Zn–MOF-74 before any exposure to humid conditions. The figure clearly shows that the simple presence of water alone does not affect the crystal structure (c), neither does high temperature (thermal decomposition point ~350 °C (ref. 55)) (b); only when combining the two (d) does the MOF disintegrate. It follows that the crystal structure is only lost when the dissociation reaction takes place, proving that the reaction products OH and H are responsible for the degradation of Zn–MOF-74.

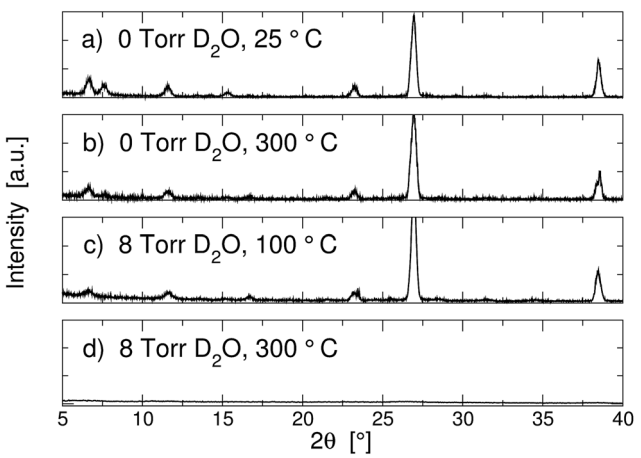

Fig. 4 (a) XRD patterns of the pristine Zn–MOF-74 before exposure to water at 25 °C. (b) XRD patterns after exposure to 300 °C for 48 hours under vacuum (less than 20 mTorr). (c) XRD patterns after exposure to 100 °C and 8 Torr of D_2O for 48 hours. (d) XRD patterns after exposure to 300 °C and 8 Torr of D_2O for 48 hours.

To further support this claim and elucidate how the H_2O, OH, and H groups affect the structure of the MOF-74 system, we use *ab initio* calculations and investigate the weakest link in the MOF-74 structure, *i.e.* the O–M bonds at the junctions between the metal centers and the linkers. Four cases will be considered: (i) the H_2O molecule is adsorbed at the metal center, (ii) the OH group is adsorbed at the metal center and one H atom is attached to the O atom of the linker. Case (iii) and (iv) correspond to the scenarios of having one OH at the metal center and one H at the O of the linker, independently. Case (i) corresponds to a water molecule adsorbed at the metal center, before any dissociation has occurred, whereas case (ii) correspond to the scenario where the water molecule has split, as indicated in Fig. 2. In the MOF-74 structure, each metal center is connected to four linkers trough their O atoms, but one linker connects *via* two O atoms so that in total each metal center is bonded to five O atoms. We will refer to these bonds as **A**, **B**, **C**, **D**, and **E**, as shown in Fig. 5. We report the O–M bond length change for cases (i)–(iv) in Table 2 for Mg–, Zn–, Co–, and Ni–MOF-74.

In the first two rows for each metal, Table 2 shows the bond length change caused by the adsorption of water on the metal center and the dissociation of this molecule into OH + H. The largest changes are highlighted in bold. Note that an excessive elongation of bonds is the precursor for breaking. Contrary to the assumption that the adsorption of H_2O on the metal centers by itself is responsible for the structural instability of MOF-74, Table 2 shows that for all cases studied (Mg–, Zn–, CO–, and Ni–MOF-74) H_2O itself has only a negligible effect on the O–M bonds compared to the reaction products OH + H. This shows once more that the instability of MOF-74 under humid conditions has its roots in the dissociation reaction at the metal sites, that produces OH and H groups, and not in the interaction of the H_2O molecule and the MOF. Note that Mg– and Co–MOF-74 are the systems that exhibit the smallest elongation in the O–M bonds, while Zn– and Ni–MOF-74 are the most affected once the $H_2O \rightarrow OH + H$ reaction takes place.

Table 2 Calculated changes in the O–M bond length [%] upon adsorption of H_2O or OH at the metal center (M-site) and the attachment of H to the oxygen of the linker (O-site, indicated in Fig. 5). Results are given for M–MOF-74 with M = Mg, Zn, Co, and Ni. Changes are reported with respect to the corresponding pristine M–MOF-74 systems; negative numbers indicate a shortening of the bond

M	M-site	O-site	A	B	C	D	E
Mg	H_2O	×	0.8	0.7	**4.2**	2.0	1.5
	OH	H	−2.3	1.0	18.9	**52.1**	1.1
	OH	×	3.1	3.1	**16.6**	8.3	1.7
	×	H	7.3	−2.9	1.8	**16.5**	−1.5
Zn	H_2O	×	0.8	3.1	**5.2**	4.1	0.2
	OH	H	−4.3	0.1	76.9	**81.9**	4.0
	OH	×	−4.0	−1.0	**74.6**	67.9	1.4
	×	H	14.9	13.4	2.6	**42.5**	5.8
Co	H_2O	×	−5.4	−9.4	**8.6**	0.7	1.9
	OH	H	−3.6	1.4	3.2	**60.8**	3.2
	OH	×	−0.3	1.5	2.4	3.6	**6.3**
	×	H	12.6	−4.9	5.7	**45.9**	−0.2
Ni	H_2O	×	6.0	5.4	−11.4	**8.8**	5.2
	OH	H	−2.0	1.5	21.5	**81.2**	−0.1
	OH	×	−2.6	1.3	19.0	**71.7**	−0.4
	×	H	11.6	5.1	−0.3	**64.6**	1.6

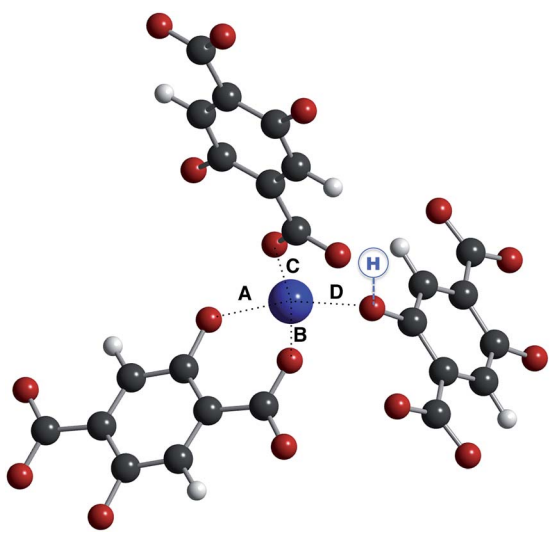

Fig. 5 O–M bonds in MOF-74. Red, black, white, and blue spheres represent O, C, H, and M atoms, respectively. The linker making bond **E** (which is very similar to bond **C**) is not shown, as it points straight out of the page.

The strong and complex effect of the reaction products OH and H combined can be disentangled by studying their individual effects. We have tabulated the elongation of the O–M bonds caused by these two groups independently in Table 2. It is particularly important to note that the water dissociation OH + H at a particular metal site, viewed from a neighboring metal side, looks like the H-only case at the O-site. In the case where we have only an OH group at the metal center, the O–Co bonds are the least affected, followed by O–Mg, O–Ni, and O–Zn bonds, in that order. However, the OH group affects the O–M bonds in different ways for each metal center and the complex interaction between the metal centers and the OH groups does not allow for a simple explanation of why some metals centers are more or less affected than others. On the other hand, the attachment of only the H group to the linker primary affects the **D** bond, see Fig. 5 and Table 2. More importantly, Table 2 shows that the elongation of this bond follows the order O–Mg < O–Zn < O–Co < O–Ni, suggesting the following explanation: in the O–M covalent bond the O pulls electrons away form the metal center. As H attaches to the O of the linker, it donates its electron to the O. In turn, O loses its ability of pulling electrons from the metal centers, weakening the **D** bond and ultimately elongating it. The described effect corresponds exactly to the concept of electronegativity. For the metals we find the following values for the Pauli electronegativity:[56] Mg (1.31) < Zn (1.65) < Co (1.88) < Ni (1.91), *i.e.* the exact same order found in the elongation of the **D** bond. We conclude that the electronegativity of the metal centers can be used as a descriptor of the MOF-74 stability under the effect of H groups attached to the linker.

Mg–MOF-74, similar to Zn–MOF-74, also has a strong catalytic activity for the water dissociation reaction—see Table 1 and

Fig. 3. One might thus assume that it also easily disintegrates in the presence of water. However, experiments confirm that its crystal structure is unaltered after being exposed to humid conditions,[39] while its CO_2 uptake capacity is significantly reduced. We understand the latter in the context of the top panel of Fig. 3; the former can be elegantly explained by looking at the changes in bond lengths. In Mg–MOF-74, even though the adsorption of H and OH has a stronger effect on the O–M bonds than the adsorption of H_2O, the elongation of these bonds is significantly smaller than in Zn–, Ni–, and Co–MOF-74, see Table 2. We can thus explain the apparent contradictory experimental finding by other authors[39–41] that Mg–MOF-74 is structurally stable even though its CO_2 uptake is significantly reduced in the presence of water. Furthermore, Liu and Co-workers[39] also pointed out that Ni–MOF-74 looses its crystal structure after exposing it to humid conditions, however, its CO_2 uptake capacity is less affected than in Mg–MOF-74. The top panel of Fig. 3 shows that the catalytic activity of Ni–MOF-74 towards the dissociation reaction is small, explaining why the CO_2 uptake capacity has a small decrease after the exposure to water. On the other hand, Table 2 shows that the H and OH groups have a large impact on the O–Ni bonds, larger than in all the other systems, explaining why the crystal structure of Ni–MOF-74 degrades easily under humid conditions.

In summary, the CO_2 reduction uptake and loss of crystal structure after MOF-74 is exposed to humid conditions are not related. Concerning the former mechanism, once MOF-74 has been exposed to water above 150 °C, the water dissociation reaction has produced the products OH (bound to the metal center) and H (bound to the oxygen of the linker). As the metal centers are now occupied by the OH groups, they become poisoned, suppressing the adsorption of new guest molecules and consequently we see a reduction in the CO_2 uptake capacity in all members of the MOF-74 family. This reduction is directly proportional to the catalytic activity of the MOF-74 towards the $H_2O \rightarrow OH + H$ reaction, which we were able to link to the radius of the metal. On the other hand, how strong the metal centers can hold on to their linkers and retain their structure after the water has dissociated is an entirely different question. Concerning this latter mechanism, we find that—depending on the electronegativity of the metal—the reaction products OH and H by themselves may now significantly elongate the O–M bonds and thus cause the loss of crystal structure. The two mechanism are related only insofar as that some water needs to dissociate in the first mechanism (responsible for the CO_2 uptake reduction) so that the second mechanism can take place (loss of crystal structure).

2.4 Suppressing water dissociation to increase MOF structural stability

With the precise knowledge of what causes the structural instability of MOF-74, we are now in a position to propose modifications of MOF-74 that might make it more water stable. According to our findings, the key element is to suppress the water dissociation reaction, such that the reaction products (OH and H) do not occur. One possible way to accomplish this is to substitute the O atom at the linker (the one where the H is attaching after the dissociation takes place) with a different atom. S is a good candidate for this purpose, as it (i) has the same number of valence electron and is thus chemically similar to O and (ii) it is less electronegative,[56] suggesting that it might have a less strong "draw" on the H from the water at the metal site. This linker modification is shown in Fig. 6. We confirm this conjecture with *ab initio* transition-state calculations,[57,58] modeling the reaction pathway for the $H_2O \rightarrow OH + H$ reaction for the original Zn–MOF-74 and the proposed S-modified Zn–MOF-74; results are plotted in Fig. 7. From this figure we see that the pristine Zn–MOF-74 has an activation barrier for the water dissociation reaction of 1.02 eV. However, the S-modified Zn–MOF-74 system has an activation barrier of 1.60 eV, which is 0.58 eV higher. From the Arrhenius equation we can estimate (assuming the same pre-exponential factor for both reactions and a temperature of 200 °C) that the rate of water dissociation in S-modified Zn–MOF-74 is only 10^{-7} of that in Zn–MOF-74, and thus essentially completely suppressed.

Unfortunately, we have not been able to experimentally verify the stability of S-modified Zn–MOF-74. When we try to synthesize the S-modified Zn–MOF-74 structure using the S ligand (H_4DSBDC), the reactants form a different structure. We believe this is because the formation of a strong bond between the hard

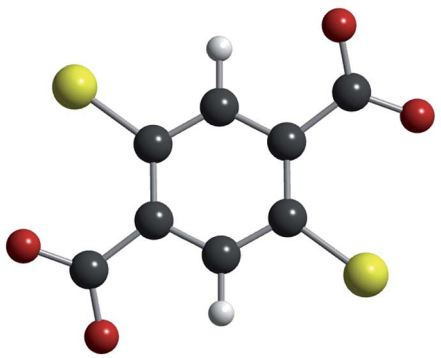

Fig. 6 S-modified linker (H_4DSBDC). Black, red, white, and yellow spheres represent C, O, H and S atoms, respectively. The S atoms occupy the position of the O atoms in the regular linker (H_4DOBDC).

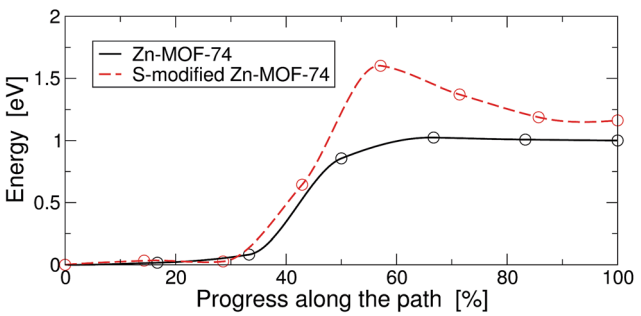

Fig. 7 Activation barrier for the water dissociation reaction $H_2O \rightarrow OH + H$ in Zn–MOF-74 and S-modified Zn–MOF-74. The barrier in the S-modified system is much higher, in effect completely suppressing this reaction and thus stabilizing the MOF.

acids, Zn^{2+}, and the soft S is difficult. On the other hand, Sun and co-workers[59] have been able to synthesize S-modified Mn–MOF-74, but this MOF also eludes experimental verification of our hypothesis, as it—with and without modification—is extremely unstable. Our experiments showed that the methanol exchanged S-modified Mn–MOF-74 sample decomposed quickly (<100 min) upon contact with air, possibly due to the oxidation of the Mn^{2+} metal centers by O_2. This, plus the small catalytic activity towards the $H_2O \rightarrow OH + H$ reaction of the Mn–MOF-74 system, prevent us from comparing the stability between the pristine and the S-modified Mn–MOF-74. Work to synthesize and confirm the stability of S-modified and other modifications that suppress the water dissociation reaction in MOF-74 is currently ongoing.

3 Summary

In this work we offer a comprehensive explanation of the crystal structure instability and CO_2 uptake reduction of MOF-74 in the presence of water. We show that water by itself has a negligible effect on the stability of the MOF crystal structure and no influence on the reduction of the CO_2 uptake, since it can be reversibly removed from the MOF. We further show that the water dissociation reaction $H_2O \rightarrow OH + H$, which is governed by the radius of the metal, is responsible for the reduction of the CO_2 gas uptake and sets the stage for the possible disintegration of the MOF. Its products, OH and H, might—depending on the metal and its electronegativity—significantly elongate the O–M bonds, which leads to the loss of the crystal structure. Future research concerning the design of water stable MOF-74 thus needs to focus on the suppression of the $H_2O \rightarrow OH + H$ reaction at the metal centers.

4 Methods

4.1 CO_2 uptake measurements and crystal-structure determination

To measure the CO_2 uptake of Zn–, Mg–, Ni–, and Co–MOF-74, each MOF-74 powder (~2 mg) was pressed onto a KBr pellet (~1 cm diameter, 1–2 mm thick). The sample was placed into a high-pressure high-temperature cell (product number P/N 5850c, Specac Ltd, UK) at the focal point compartment of an infrared spectrometer (Nicolet 6700, Thermo Scientific, US). The samples were activated under vacuum at 180 °C for at least 4 hours; when humidity levels were reduced, the sample was cooled down to room temperature. 6 Torr of CO_2 was loaded into the cell for a period of 30 minutes, spectra were recorded as a function of time during the adsorption process to evaluate the CO_2 uptake before water exposure. Evacuation of CO_2 for a period of 30 minutes, reaching a pressure below 200 mTorr, was done prior to the increase of temperature at 100 °C and 200 °C (two sets of experiments); at this point, 8 Torr of heavy water (D_2O) was loaded into the cell for a period of 20 minutes, spectra were recorded. Desorption of water was done at 150 °C for 5 hours to assure water removal. The sample was cooled back down to room temperature to evaluate the CO_2 uptake after water exposure under the same conditions (6 Torr of CO_2 for 30 minutes).

The structural instability in the presence of water was investigated in detail for Zn–MOF-74. To this end, Zn–MOF-74 pellets were fabricated and their crystalline structure was characterized by X-ray diffraction (Rigaku Ultima III XRD) before and after water exposure. Samples were subjected to a pressure of 8 Torr of water at 100 °C and 300 °C for two days. As a control experiment, the same was done without water at room temperature (25 °C) and high temperature (300 °C).

4.2 *Ab initio* simulations

Ab initio calculations were performed at the DFT level with the VASP code.[60] We used projector augmented wave (PAW) pseudopotentials[61] and a plane-wave expansion with a kinetic-energy cutoff of 600 eV. Due to the important van der Waals interaction between the metal centers of the MOF and the guest molecules, we used the vdW-DF exchange-correlation functional.[62–65] Due to the large dimensions of the unit cell, only the Γ-point was sampled.

We started from the experimental rhombohedral structure of Zn–, Mg–, Ni–, and Co–MOF-74 with 54 atoms in its primitive cell and space group $R\bar{3}$.[31] Then, the positions of the atoms and cell were relaxed until the forces were less than 1 meV $Å^{-1}$. These systems were used to calculate the oxygen–metal (O–M) bond elongations caused by H_2O, OH, and H groups. Again, in all these cases, the atoms were relaxed until the forces were less than 1 meV $Å^{-1}$. To model the $H_2O \rightarrow OH + H$ reaction we used a transition-state search algorithm, *i.e.* the climbing-image nudged-elastic band method.[57,58]

Acknowledgements

This work was entirely supported by Department of Energy Grant No. DE–FG02–08ER46491. It further used resources of the Oak Ridge Leadership Computing Facility at Oak Ridge National Laboratory, which is supported by the Office of Science of the Department of Energy under Contract DE–AC05–00OR22725.

References

1 J. Liu, P. K. Thallapally, B. P. McGrail, D. R. Brown and J. Liu, *Chem. Soc. Rev.*, 2012, **41**, 2308–2322.
2 L. J. Murray, M. Dinca and J. R. Long, *Chem. Soc. Rev.*, 2009, **38**, 1294–1314.
3 J.-R. Li, Y. Ma, M. C. McCarthy, J. Sculley, J. Yu, H.-K. Jeong, P. B. Balbuena and H.-C. Zhou, *Coord. Chem. Rev.*, 2011, **255**, 1791–1823.
4 S. Qiu and G. Zhu, *Coord. Chem. Rev.*, 2009, **253**, 2891–2911.
5 N. Nijem, H. Wu, P. Canepa, A. Marti, K. J. Balkus, T. Thonhauser, J. Li and Y. J. Chabal, *J. Am. Chem. Soc.*, 2012, **134**, 15201–15204.
6 K. Lee, J. D. Howe, L.-C. Lin, B. Smit and J. B. Neaton, *Chem. Mater.*, 2015, **27**, 668–678.

7 D. Zhao, D. Yuan and H.-C. Zhou, *Energy Environ. Sci.*, 2008, **1**, 222–235.
8 N. L. Rosi, J. Eckert, M. Eddaoudi, D. T. Vodak, J. Kim, M. O'Keeffe and O. M. Yaghi, *Science*, 2003, **300**, 1127–1129.
9 H. Wu, Q. Gong, D. H. Olson and J. Li, *Chem. Rev.*, 2012, **112**, 836–868.
10 Y. He, W. Zhou, G. Qian and B. Chen, *Chem. Soc. Rev.*, 2014, **43**, 5657–5678.
11 L. E. Kreno, K. Leong, O. K. Farha, M. Allendorf, R. P. Van Duyne and J. T. Hupp, *Chem. Rev.*, 2012, **112**, 1105–1125.
12 C. Serre, C. Mellot-Draznieks, S. Surblé, N. Audebrand, Y. Filinchuck and G. Férey, *Science*, 2007, **315**, 1828–1831.
13 M. D. Allendorf, R. J. T. Houk, L. Andruskiewicz, A. A. Talin, J. Pikarsky, A. Choundhury, K. A. Gall and P. J. Hensketh, *J. Am. Chem. Soc.*, 2008, **130**, 14404–14405.
14 J.-C. Tan and A. K. Cheetham, *Chem. Soc. Rev.*, 2011, **40**, 1059–1080.
15 Z. Hu, B. J. Deibert and J. Li, *Chem. Soc. Rev.*, 2014, **43**, 5815–5840.
16 T. Uemura, N. Yanai and S. Kitagawa, *Chem. Soc. Rev.*, 2009, **38**, 1228–1236.
17 M. J. Vitorino, T. Devic, M. Tromp, G. Férey and M. Visseaux, *Macromol. Chem. Phys.*, 2009, **210**, 1923–1932.
18 M. D. Allendorf, C. A. Bauer, R. K. Bhakta and R. Houk, *Chem. Soc. Rev.*, 2009, **38**, 1330–1352.
19 K. A. White, D. A. Chengelis, K. A. Gogick, J. Stehman, N. L. Rosi and S. Petoud, *J. Am. Chem. Soc.*, 2009, **131**, 18069–18071.
20 S. Bordiga, C. Lamberti, G. Ricchiardi, L. Regli, F. Bonino, A. Damin, K.-P. Lillerud, M. Bjorgen and A. Zecchina, *Chem. Commun.*, 2004, 2300–2301.
21 M. Kurmoo, *Chem. Soc. Rev.*, 2009, **38**, 1353–1379.
22 P. Horcajada, T. Chalati, C. Serre, B. Gillet, C. Sebrie, T. Baati, J. Eubank, D. Heurtaux, P. Clayette, C. Kreuz, J.-S. Chang, Y. Hwang, V. Marsaud, P.-N. Bories, L. Cynober, S. Gil, G. Férey, P. Couvreur and R. Gref, *Nat. Mater.*, 2010, **9**, 172–178.
23 A. Stroppa, P. Jain, P. Barone, M. Marsman, J. M. Perez-Mato, A. K. Cheetham, H. W. Kroto and S. Picozzi, *Angew. Chem., Int. Ed.*, 2011, **50**, 5847–5850.
24 A. Stroppa, P. Barone, P. Jain, J. M. Perez-Mato and S. Picozzi, *Adv. Mater.*, 2013, **25**, 2284–2290.
25 D. Di Sante, A. Stroppa, P. Jain and S. Picozzi, *J. Am. Chem. Soc.*, 2013, **135**, 18126–18130.
26 C.-D. Wu and W. Lin, *Angew. Chem., Int. Ed.*, 2007, **46**, 1075–1078.
27 J. Lee, O. K. Farha, J. Roberts, K. A. Scheidt, S. T. Nguyen and J. T. Hupp, *Chem. Soc. Rev.*, 2009, **38**, 1450–1459.
28 R.-Q. Zou, H. Sakurai and Q. Xu, *Angew. Chem., Int. Ed.*, 2006, **45**, 2542–2546.
29 I. Luz, F. X. L. i. Xamena and A. Corma, *J. Catal.*, 2010, **276**, 134–140.
30 Y. Liu, H. Kabbour, C. M. Brown, D. A. Neumann and C. C. Ahn, *Langmuir*, 2008, **24**, 4772–4777.
31 W. Zhou, H. Wu and T. Yildirim, *J. Am. Chem. Soc.*, 2008, **130**, 15268–15269.
32 H. Wu, J. M. Simmons, G. Srinivas, W. Zhou and T. Yildirim, *J. Phys. Chem. Lett.*, 2010, **1**, 1946–1951.
33 P. D. C. Dietzel, R. E. Johnsen, H. Fjellvag, S. Bordiga, E. Groppo, S. Chavan and R. Blom, *Chem. Commun.*, 2008, 5125–5127.
34 S. R. Caskey, A. G. Wong-Foy and A. J. Matzger, *J. Am. Chem. Soc.*, 2008, **130**, 10870–10871.
35 L. Valenzano, B. Civalleri, S. Chavan, G. T. Palomino, C. O. Arean and S. Bordiga, *J. Phys. Chem. C*, 2010, **114**, 11185–11191.
36 H. Wu, W. Zhou and T. Yildirim, *J. Am. Chem. Soc.*, 2009, **131**, 4995–5000.
37 A. C. Kizzie, A. G. Wong-Foy and A. J. Matzger, *Langmuir*, 2011, **27**, 6368–6373.
38 T. Remy, S. A. Peter, S. Van der Perre, P. Valvekens, D. E. De Vos, G. V. Baron and J. F. M. Denayer, *J. Phys. Chem. C*, 2013, **117**, 9301–9310.
39 J. Liu, A. I. Benin, A. M. B. Furtado, P. Jakubczak, R. R. Willis and M. D. LeVan, *Langmuir*, 2011, **27**, 11451–11456.
40 P. M. Schoenecker, C. G. Carson, H. Jasuja, C. J. J. Flemming and K. S. Walton, *Ind. Eng. Chem. Res.*, 2012, **51**, 6513–6519.
41 J. B. DeCoste, G. W. Peterson, B. J. Schindler, K. L. Killops, M. A. Browe and J. J. Mahle, *J. Mater. Chem. A*, 2013, **1**, 11922–11932.
42 N. C. Burtch, H. Jasuja and K. S. Walton, *Chem. Rev.*, 2014, **114**, 10575–10612.
43 Y. Li, Z. Ju, B. Wu and D. Yuan, *Cryst. Growth Des.*, 2013, **13**, 4125–4130.
44 K. Tan, N. Nijem, P. Canepa, Q. Gong, J. Li, T. Thonhauser and Y. J. Chabal, *Chem. Mater.*, 2012, **24**, 3153–3167.
45 S. Han, Y. Huang, T. Watanabe, S. Nair, K. S. Walton, D. S. Sholl and J. C. Meredith, *Microporous Mesoporous Mater.*, 2013, **173**, 86–91.
46 W.-Y. Gao, R. Cai, T. Pham, K. A. Forrest, A. Hogan, P. Nugent, K. Williams, L. Wojtas, R. Luebke, L. J. Weselinski, M. J. Zaworotko, B. Space, Y.-S. Chen, M. Eddaoudi, X. Shi and S. Ma, *Chem. Mater.*, 2015, **27**, 2144–2151.
47 J. B. Decoste, G. W. Peterson, M. W. Smith, C. A. Stone and C. R. Willis, *J. Am. Chem. Soc.*, 2012, **134**, 1486–1489.
48 D. Ma, Y. Li and Z. Li, *Chem. Commun.*, 2011, **47**, 7377–7379.
49 Y. Jiao, C. R. Morelock, N. C. Burtch, W. P. Mounfield III, J. T. Hungerford and K. S. Walton, *Ind. Eng. Chem. Res.*, 2015, **54**, 12408–12414.
50 S. S. Han, S.-H. Choi and A. C. T. van Duin, *Chem. Commun.*, 2010, **46**, 5713–5715.
51 K. Tan, S. Zuluaga, Q. Gong, P. Canepa, H. Wang, J. Li, Y. J. Chabal and T. Thonhauser, *Chem. Mater.*, 2014, **26**, 6886–6895.
52 K. Tan, N. Nijem, Y. Gao, S. Zuluaga, J. Li, T. Thonhauser and Y. J. Chabal, *CrystEngComm*, 2015, **17**, 247–260.
53 E. Clementi and D. L. Raimondi, *J. Chem. Phys.*, 1963, **38**, 2686–2689.
54 P. Canepa, C. A. Arter, E. M. Conwill, D. H. Johnson, B. A. Shoemaker, K. Z. Soliman and T. Thonhauser, *J. Mater. Chem. A*, 2013, **1**, 13597–13604.

55 P. D. Dietzel, R. E. Johnsen, R. Blom and H. Fjellvåg, *Chem.–Eur. J.*, 2008, **14**, 2389–2397.
56 A. L. Allred, *J. Inorg. Nucl. Chem.*, 1961, **17**, 215–221.
57 G. Henkelman, B. P. Uberuaga and H. Jónsson, *J. Chem. Phys.*, 2000, **113**, 9901–9904.
58 G. Henkelman and H. Jónsson, *J. Chem. Phys.*, 2000, **113**, 9978–9985.
59 L. Sun, T. Miyakai, S. Seki and M. Dinca, *J. Am. Chem. Soc.*, 2013, **135**, 8185–8188.
60 G. Kresse and J. Furthmüller, *Phys. Rev. B: Condens. Matter Mater. Phys.*, 1996, **54**, 11169–11186.
61 G. Kresse and D. Joubert, *Phys. Rev. B: Condens. Matter Mater. Phys.*, 1999, **59**, 1758–1775.
62 T. Thonhauser, S. Zuluaga, C. A. Arter, K. Berland, E. Schröder and P. Hyldgaard, *Phys. Rev. Lett.*, 2015, **115**, 136402.
63 K. Berland, V. R. Cooper, K. Lee, E. Schröder, T. Thonhauser, P. Hyldgaard and B. I. Lundqvist, *Rep. Prog. Phys.*, 2015, **78**, 066501.
64 D. C. Langreth, B. I. Lundqvist, S. D. Chakarova-Käck, V. R. Cooper, M. Dion, P. Hyldgaard, A. Kelkkanen, J. Kleis, L. Kong, S. Li, P. G. Moses, E. D. Murray, A. Puzder, H. Rydberg, E. Schröder and T. Thonhauser, *J. Phys.: Condens. Matter*, 2009, **21**, 084203.
65 T. Thonhauser, V. R. Cooper, S. Li, A. Puzder, P. Hyldgaard and D. C. Langreth, *Phys. Rev. B: Condens. Matter Mater. Phys.*, 2007, **76**, 125112.